J. Fluid Mech. (1976), *vol.* 77, *part* 1, *pp.* 63–80
Printed in Great Britain

Experiments on the stability of liquid films adjacent to supersonic boundary layers

By WILLIAM S. SARIC, ALI H. NAYFEH and SPYRIDON G. LEKOUDIS

Department of Engineering Science and Mechanics, Virginia Polytechnic Institute and State University, Blacksburg

(Received 9 February 1976)

The stability of liquid films adjacent to supersonic streams was investigated experimentally and compared with analytical results. Linear theories predict that films adjacent to supersonic streams are much more unstable than those adjacent to subsonic streams. However, our supersonic experimental observations indicated that the liquid film was stable with no entrainment under all test conditions. These conditions included laminar and turbulent boundary layers, a variation in the liquid Reynolds number (based on flow rate) from 1 to 200 and a variation in the free-stream unit Reynolds number from $1{\cdot}6 \times 10^6$ m^{-1} to $110{\cdot}0 \times 10^6$ m^{-1}. These experimental observations can be explained by nonlinear theories, which predict that linear unstable disturbances do not grow indefinitely but achieve steady-state amplitudes in the supersonic case. The different aspects of the observed wave behaviour such as frequency, wavelength and amplitude are discussed and compared with previous experimental observations and the nonlinear theories.

1. Introduction

The advent of new, sophisticated missions for re-entry vehicles has generated a renewed interest in transpiration cooling as a protective system maintaining re-entry vehicle geometry and structural integrity under the effects of aerodynamic heating. The technique consists of injecting a liquid coolant in the stagnation region and allowing the liquid to be swept back over the body, providing a protective liquid layer. Thus, of particular importance in transpiration cooling is estimation of the liquid removal by either entrainment or evaporation. To estimate the amount of liquid entrained by the gas, one needs to determine the stability characteristics of the liquid/gas interface. To estimate the amount of liquid removal by evaporation, one needs to know the roughness characteristics of the interface, i.e. interface wave characteristics such as the wavelength and amplitude. These estimates are also important because the multi-phase flow near the interface might increase the degree of turbulent transport (in the case of turbulent gas boundary layers) and cause transition in the liquid film. This phenomenon is called volumetric boiling. Moreover, for maximum protection, the dominant liquid loss mechanism must be evaporation.

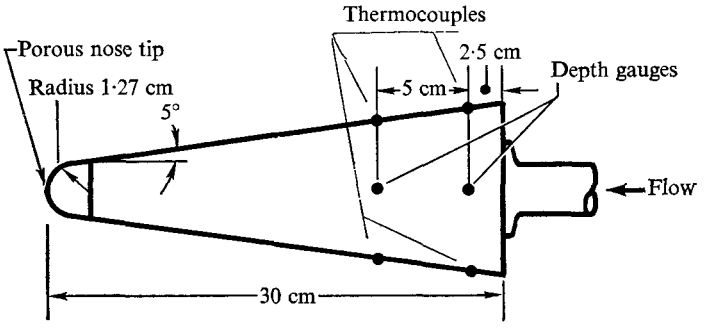

FIGURE 1. Experimental test model.

Early experiments with a nearly incompressible, turbulent gas flow (Gater & L'Ecuyer 1971) showed that the dominant liquid removal mechanism is entrainment of the liquid by the gas. In evaluating the concept of transpiration cooling, early investigators extrapolated the incompressible results to the supersonic case, in spite of the different stability mechanisms, and arrived at a negative conclusion.

Experiments with a supersonic flow were first conducted by Saric & Marshall (1971). They showed a stable liquid layer in this case. However, they only considered laminar boundary layers. As part of an independent, parallel effort, Gold (1973) conducted experiments with a turbulent boundary layer. These experiments are described in the present paper in some detail and are compared with the present experiments.

A systematic approach was planned for the prediction of the stability characteristics and observed wavelengths and corresponding wave speeds and amplitudes on the surface of a liquid film adjacent to a supersonic stream. The experiments included laminar and turbulent boundary layers, and in some cases the entrainment parameters matched those which Gater & L'Ecuyer (1971) obtained in their subsonic experiments. The experimental observations are compared with the analytical results.

2. Description of experiments

The experiments were conducted in New York University's hypersonic wind tunnel at a free-stream Mach number of 6. This tunnel is an intermittent blow-down-to-vacuum type. It is electrically heated. The test section is axisymmetric, 60 cm long and 30 cm in diameter. Test times were limited to 20 s with a frequency of one per hour.

Models and instrumentation

Two models were used for the experiments. Figure 1 is a sketch of the sphere–cone model with a nose tip 2·54 cm in diameter. The nose tip is removable and is made of porous stainless-steel manufactured by a special process by McDonnell-Douglas. Tips with permeabilities of $3{\cdot}2 \times 10^{-9}$ cm^2 and $0{\cdot}65 \times 10^{-9}$ cm^2 were used. The variation of permeability was measured to be less than 7 % over the entire

tip. The other model had a hemispherical tip 1·27 cm in diameter attached as an extension of the cone so that the total length of the model was increased to 38 cm, thus doubling the effective length for the pressure distribution.

The liquid was expelled through the tips by means of a high-pressure expulsion system connected to the base of the model through the sting. The expulsion system consisted of a reservoir, filters, pressure monitoring equipment and flow-rate metering equipment. The fluid was displaced by a single positive movement of a piston in the reservoir. Pressure drops across the tip were held between 50 and 100 atm to prevent tunnel pressure fluctuations and the spherical pressure distribution from affecting the flow rates. The flow rates were measured by recording the pressure drops across orifices that were calibrated for fluids of different viscosities. The liquid flow rate, the wind-tunnel conditions (such as stagnation and static pressures and total temperature) and the measured liquid temperatures were simultaneously recorded as functions of time on the tunnel data system.

The interface response was photographed with high-speed 16 mm and 35 mm cameras. The cameras observed the model through a side window in the tunnel in the presence of top, bottom and side lighting provided by high-intensity tungsten lamps whose energy totalled 7 kW. A 35 mm Photosonics camera, pin-registered at 300 frame/s with a fine-grain black-and-white film, recorded the details of the wave motion on the model. By employing timing marks on the film as reference times and the nose tip as a reference length, we used a Boscar film reader coupled to a card punch and desk calculator to determine the wave velocities and wavelengths from the motion-picture film. A 16 mm HiCam camera, operating at 1000–3000 frame/s, was used to detect any high frequency phenomenon that might be present. Since the quality of the data obtained by this equipment was not as good as that from the 35 mm camera, these data were only interpreted for selected cases. A 16 mm Millican camera, pin-registered at 400 frame/s with colour film, was used to back up the other two cameras. Wavelength and wave-speed data were selected from those motion pictures and compared with the data from the 35 mm camera as an additional check.

Spark microphotographs were taken of the wave patterns by using a specially built-up lens system. By collimating and focusing the light from a spark source across the edge of the cone, photographs were taken of the wave profiles as they moved across the cone. This was also done to detect liquid drops in the gas boundary layer. The spark was generated by a capacitor discharge and had a measured duration of 3 μs. The source was at the focus of a 25 cm diameter paraboloidal collimating mirror which directed the beam to a series of 25 cm diameter focusing lenses, which in turn exposed a $10 \times 12{\cdot}5$ cm photographic plate. A 7·3 image magnification was achieved on the photographic film and magnifications of over 100 times were possible with an enlarger.

Schlieren photography was also used for selected tests by employing another condensing lens system with the spark source. No secondary shocks as a result of the liquid injection, waves or entrainment were observed with this system.

Four copper–alumel thermocouples were located on the surface of the test model to record the liquid temperature during the test. These temperatures were used as reference points to measure the viscosity of the liquid after the tests.

The depth of the liquid and the waves superposed on the liquid/gas interface were measured by two 'end-effect' capacitance gauges similar to those developed by Nachtsheim & Seegmiller (1968, private communication) and Marshall & Tiederman (1972). The gauges consisted of two small (0·22 mm wide) plates embedded in a dielectric pod and mounted on the model parallel to the surface so as not to interfere with the liquid flow. These gauges were connected by means of a doubly shielded triaxial cable to two 100 kHz capacitance bridges whose resolution was $0{\cdot}1 \times 10^{-12}$ F with a frequency response of 10 kHz. The bridges were balanced for no liquid; the presence of the liquid thus altered their capacitance, unbalancing them; the imbalances were converted to voltages; and the voltages were recorded on FM tape. The inner shield of the cable had the same potential as the bridge transformer, and thus minimized the inner conductor to outer shield shunt capacitance. This system was capable of measuring small changes in capacitance associated with small changes in liquid thickness. Care was taken during the tests to balance the gauge at room temperature and to delay the photographic lamps until liquid coverage was initiated.

A four-channel Ampex model FR 1300 tape recorder, using a multiplexer for the different input signals, was used to record the outputs of the gauges. A 6 s steady-state data sample was chosen and digitized at 100 μs intervals. Thus a large enough data sample was obtained to analyse fluctuations in the kilohertz range.

The gauges were calibrated by placing measured quantities of liquid over each gauge and measuring the voltage as a function of depth. During this post-test calibration, the gauges were balanced at room temperature and measurements were made with samples of the test liquid at the measured test temperature. This minimized any error caused by the temperature sensitivity of the gauges and thus eliminated the source of the error present in the Marshall & Tiederman measurements.

Test conditions

Tests on a dry model were conducted prior to the liquid tests in order to evaluate the gas-flow conditions. This model was a thin-skinned (0·6 mm) sphere–cone with the same dimensions as the model shown in figure 1. Twenty pressure taps and eighteen thermocouples embedded in the surface of the model were used to record the surface pressure and heat transfer for the different tunnel test conditions. These data were used as input to boundary-layer/liquid-layer computer codes to calculate the other properties of the flow field and to determine whether the boundary layer was laminar or turbulent. On the basis of this information, two tunnel conditions were chosen to produce laminar boundary layers with conditions similar to those of Saric & Marshall (1971) and two conditions were chosen to produce turbulent boundary layers where the entrainment parameter of Gater & L'Ecuyer (1971) is large. These conditions are shown in table 1. The values quoted are nominal values while calculations were based on whatever conditions were measured during the tests. Conditions I and II corresponded to laminar boundary layers and conditions III and IV corresponded to turbulent boundary layers as determined by the heat-transfer data from the thin-skinned

Condition	I	II	III	IV
Mach number (free-stream)	6	6	6	6
Total pressure (atm)	6	15	100	130
Total temperature (°K)	500	500	500	500
Reynolds number ($m^{-1} \times 10^{-6}$)	1·6	4	85	110

TABLE 1. Tunnel test conditions

model. The Stanton-number variation as a function of Reynolds number over the body followed the conventional patterns of laminar and turbulent boundary layers and clearly indicated the differences among the test conditions. These data compared very well with the data of Muir & Trujillo (1972, 1974), which were obtained under similar circumstances.

The use of the dry model to estimate the gas-flow properties over a model with a liquid film was justified *a posteriori* using the measurements of the liquid characteristics. The liquid thicknesses varied from 0·002 cm to 0·05 cm, so that the ratio of the maximum liquid depth to the minimum cone diameter was 2 %, while the maximum wave amplitude was less than 8 % of the liquid depth. The liquid did not significantly change the shape of the model and the wave amplitudes, which varied from 0·0006 to 0·004 cm, were considered small. Thus it was assumed that the mean-flow characteristics were unaffected by the liquid film. It is not known at this time how the laminar, transitional or turbulent nature of the boundary layer was affected by the flow being over a compliant surface.

The measured pressure distributions compared very well with the calculations made with the NASA–Ames inviscid flow-field code. These data were used to calculate the properties of the gas boundary layer with the BLIMP computer code developed by Kendall & Bartlett (1972) and Anderson & Kendall (1969). The liquid properties, such as depth and interface velocity, were calculated using the BLIMPL program developed by Grose & Kendall (1970).

BLIMPL is a non-similar variable-property, boundary-layer solver based on BLIMP. It is modified for liquid layers such as those found in transpiration-cooling systems. The air-over-water calculations were made by first running BLIMP under gas-over-water conditions where quasi-steady equilibrium was assumed between the liquid and the gas at the interface. The interfacial shear and mass transfer, along with the equilibrium temperature, were calculated. These results were then used as input to BLIMPL, which in turn calculated the velocity and temperature distributions in the liquid. Depending on the wall conditions of the liquid and the amount of blowing, an iterative procedure was carried out between the two programs to get the convergent results. In the results that follow, only nominal values of the shear stress are quoted. However, the other calculated properties of the liquid were based on the actual values measured during a particular test.

Mass entrainment due to mechanical removal of the liquid was not included in any of these calculations because the present experiments as well as those of Gold (1973) showed that it does not exist in the supersonic case.

The Reynolds number of the liquid, based on interface velocity U and liquid

Fluid	Nominal ratio of water to glycerin	Density (g/ml)	Nominal viscosity (cP)
A	100 : 0	1·000	1
B	40 : 60	1·143	7
C	25 : 75	1·186	15

TABLE 2. Test liquids

depth h, was varied by changing the flow rate for any particular fluid. This Reynolds number is given by $R = Uh/\nu = Q/(\pi r_c \nu)$, where Q is the volumetric flow rate of the liquid, ν is the kinematic viscosity and r_c is the local cone radius. This assumes, of course, a linear velocity profile.

The viscosity of the liquid was also varied in order to achieve an even wider range of depths and Reynolds numbers. Water and two different water–glycerin mixtures were used. They are listed in table 2. The water–glycerin percentages and the viscosities are nominal, although the actual measured values were used in the calculations. The viscosities and densities were measured from samples of each test fluid at the measured test temperatures. In all cases, blue, green or black dye was added to the mixture to provide a better contrast for the photographic film. The variation in the surface tension caused by the addition of the dye was not measured and not included in the data. It is well known that in the case of long waves, such as those which existed in these experiments, the stability criteria are relatively insensitive to the variation of the liquid surface tension. Therefore the use of nominal surface-tension values was considered acceptable.

The test matrix is shown in table 3 and includes the range of liquid parameters of Saric & Marshall (1971) and Gold (1973). This table contains the actual values of the shear stress, viscosity and temperature. Runs with multiple depth-gauge channels were duplicate runs to check repeatability of the tests. The aft gauge failed after run 39 and only the forward gauge was used for data acquisition in subsequent runs.

Test procedure

The model was rigidly mounted in the tunnel and was in equilibrium with room temperature. The electronics of the depth gauges and the liquid flow were started first, and at the first evidence of liquid emerging from the tip, the wind-tunnel flow was initiated. This procedure was adopted to prevent damage to the tip due to 'dusting' from the air flow. Within 3 s, steady-state air and liquid conditions were reached. Except for the case of very viscous liquids, the model was already covered by this time. The high intensity lamps and the cameras were then turned on for 10 s, after which they were shut down and the spark photographs were taken.

Run	Depth-gauge channel	Temperature (°K)	Viscosity [(cm²/s) × 10²]	Reynolds number $R = Q/\pi R_c \nu$	Tunnel stagnation pressure (atm)	$C_f(M^2-1)^{\frac{1}{2}}$	Edge Mach number	Gas shear stress (dyne/cm²)	Liquid flow rate (ml/s)	Calculated liquid depth (cm × 100)	Calculated interface velocity (cm/s)
					Fluid B						
15	F1	—	15·0	12·7	16	0·0023	3·04	135	16·82	4·92	38·7
	A1	—	12·0	12·5		0·0022	3·08	120		4·14	36·2
16	F2, F3†	282	15·5	12·3	7	0·0033	3·08	90	16·82	6·13	31·1
	A2, A3	281	16·0	9·4		0·0033	3·15	80		5·86	25·6
17	F4	294	10·0	10·0	16	0·0022	3·04	135	8·8	2·91	34·4
	A4	301	8·0	9·8		0·0022	3·08	120		2·44	32·1
18	F5, F6†	292	13·8	13·9	100	0·0037	3·21	1700	16·82	1·33	144·0
	A5, A6	295	11·7	12·9		0·0037	3·31	1600		1·12	134·0
19	F7	292	12·6	7·9	100	0·0037	3·21	1700	8·8	0·918	108·0
	A7	308	7·3	10·8		0·0037	3·31	1600		0·641	123·0
20	F8	294	11·0	9·1	7	0·0033	3·08	90	8·8	3·74	26·8
	A8	297	9·6	8·2		0·0033	3·15	80		3·29	24·0
21	F9	284	15·5	3·2	16	0·0022	3·04	135	4·3	2·55	19·4
	A9	306	7·7	5·0		0·0022	3·08	120		1·68	22·9
22	F10	284	15·5	6·3	16	0·0022	3·04	135	8·80	3·58	27·3
	A10	291	12·3	6·4		0·0022	3·08	120		3·04	25·9
23	F11	287	15·1	6·6	100	0·0037	3·21	1700	8·80	1·01	99·1
	A11	293	12·6	6·2		0·0037	3·31	1600		0·839	93·2
24	F12, F13†	300	9·1	5·4	100	0·0037	3·21	1700	4·3	0·548	89·6
	A12, A13	309	6·7	5·7		0·0037	3·31	1600		0·428	89·3
					Fluid C						
30	F14	317	12·0	3·2	16	0·0022	3·04	135	3·42	2·01	19·1
	A14	330	10·0	3·06		0·0022	3·08	120		1·74	17·6
31	F15	307	22·2	1·16	7	0·0033	3·08	90	2·25	2·74	9·38
	A15	314	17·0	1·19		0·0033	3·15	80		2·26	8·96
32	F16	308	21·1	0·862	16	0·0022	3·04	135	1·6	1·84	9·91
	A16	314	17·0	0·842		0·0022	3·08	120		1·55	9·23
33	F17	314	17·0	2·29	100	0·0037	3·21	1700	3·42	0·679	57·3
	A17	324	13·0	2·35		0·0037	3·31	1600		0·543	56·3
34	F18, F19†	332	9·15	2·0	100	0·0037	3·21	1700	1·6	0·342	53·5
	A18, A19	—	9·0	2·0		0·0037	3·31	1600		0·347	51·9

					Fluid A						
35	F20	284	1·27	80·0	7	0·003	3·08	82	8·94	1·25	81·0
	A20	283	1·31	61·0		0·003	3·12	73		1·20	66·7
36	F21	279	1·49	68·2	16	0·002	3·04	125	8·94	1·10	92·3
	A21	293	1·0	80·0		0·002	3·08	120		0·816	97·8
37	F22	280	1·47	138·0	16	0·002	3·04	125	17·9	1·54	131·0
	A22	291	1·1	145·0		0·002	3·08	120		1·21	132·0
38	F23	282	1·37	135·0	16	0·002	3·04	125	16·3	1·42	130·0
	A23	294	1·01	144·0		0·002	3·08	120		1·11	131·0
39	F24	289	1·12	45·5	100	0·0035	3·21	1500	4·47	0·195	261·0
	A24	338	—	—		0·0035	3·31	1500			
40	F25	284	1·27	80·0	100	0·0035	3·04	1500	8·94	0·293	346·0
41	F26	285	1·22	167·0	100	0·0035	3·04	1500	17·9	0·407	500·0
42	F27	281	1·29	78·8	100	0·0035	3·04	1500	8·94	0·296	344·0
43	F28	289	1·12	90·7	130	0·0035	3·21	1800	8·94	0·251	404·0
45	F29	287	1·19	171·0	130	0·0035	3·21	1700	17·9	0·377	539·0
46	F30, 31, 32†	291	1·1	267·0	130	0·0035	3·21	1700	25·8	0·436	674·0
47	F33	293	1·0	102·0	130	0·0035	3·21	1700	8·94	0·245	416·0
48	F34, F35†	288	1·17	174·0	130	0·0035	3·21	1700	17·9	0·374	544·0
49	F36	285	1·22	167·0	100	0·0035	3·04	1500	17·9	0·407	500·0
50	F37	293	1·01	50·3	130	0·0035	3·21	1700	4·47	0·174	292·0
					Fluid B						
52	F38	292	11·0	9·1	130	0·0037	3·20	1900	8·8	0·814	123·0
53	F39	293	8·4	5·8	130	0·0037	3·20	1900	4·3	0·496	98·2
54	F40	284	13·8	7·2	16	0·0022	3·04	135	8·8	3·41	29·2
55	F41	289	12·2	8·2	16	0·0022	3·04	135	8·8	3·21	31·1

† Repeated tests

TABLE 3. Calculated test conditions (F and A denote forward and aft depth-gauge channels respectively)

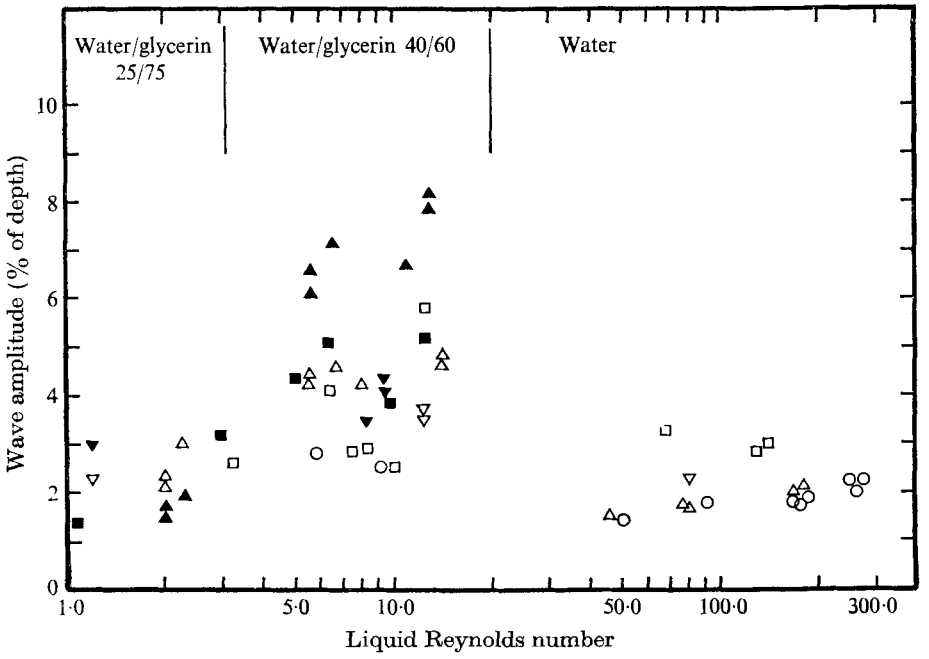

FIGURE 4. Variation of wave amplitude with Reynolds number and flow properties. Open symbols, from forward depth gauge; closed symbols, from aft gauge. Laminar case: ▼, τ = 80 dynes/cm^2; ▽, τ = 90; ■, τ = 120; □, τ = 135. Turbulent case: ▲, τ = 1600; △, τ = 1700; ○, τ = 1900.

3. Experimental results

Waves were observed to form on the surface of a stable liquid film. This was true for all liquid Reynolds numbers, all fluids and for both laminar and turbulent boundary layers. An example of this is shown in figure 2 (plate 1). One observes a regular almost axisymmetric wave pattern moving backwards over the body. This test used air over water with a laminar boundary layer and a liquid Reynolds number of 80. The waves moved faster than the interface velocity, which is a sufficient condition for externally excited disturbances.

Three-dimensional waves that resembled scalloped patterns were also observed. These waves were similar to those observed by Saric & Marshall (1971) on a flat plate and by Chapman & Larson (1962) on tektites. These waves did not propagate transverse to the mean flow but propagated parallel to it, as if a stationary transverse wave was superposed on the moving wave. No measurements were made of the transverse waves. The three-dimensional waves were not the so-called 'cross-hatched' waves, which are parallel to Mach lines. We did not observe during these tests any disturbance that was parallel to or propagated along Mach lines.

The spark microphotograph shown in figure 3 (plate 2) is typical of many of the photographs of the wave profiles. In this case, the boundary layer was turbulent and flowed over a very viscous water–glycerin mixture. The runs with a laminar boundary layer were characterized by much thicker layers and steeper wave fronts very like a saw-tooth. No entrainment was observed and the mean

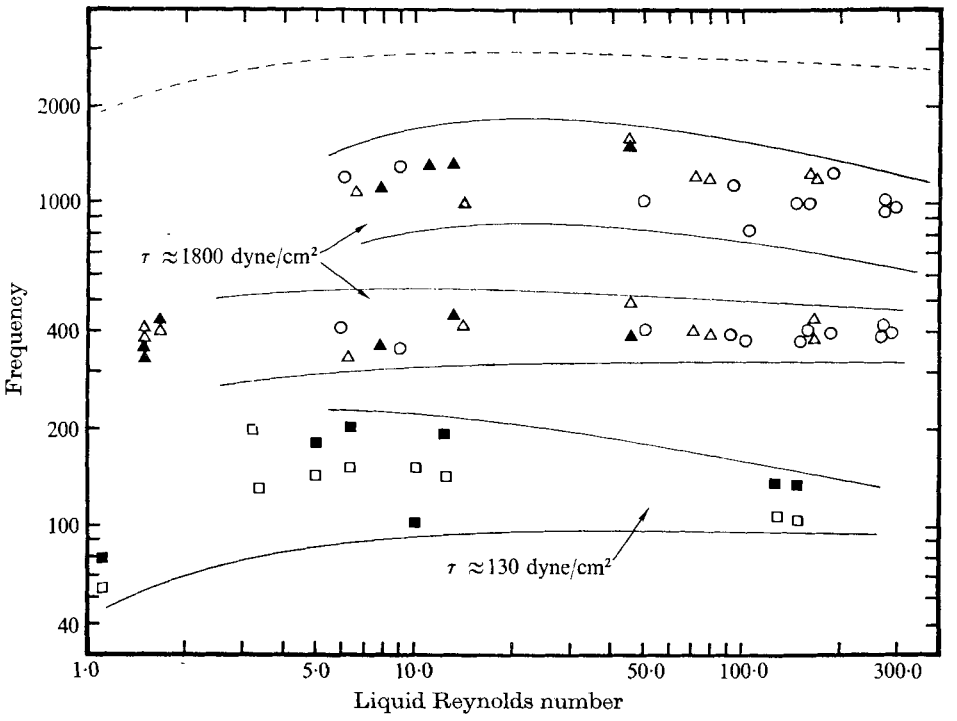

FIGURE 5. Variation of frequency with Reynolds number and flow properties.

depth measured by the capacitance gauge was approximately equal to that predicted by the boundary-layer code assuming no entrainment. Furthermore, the r.m.s. amplitude *decreased* as the mean shear stress of the gas increased for high liquid Reynolds numbers. This is related to the nonlinear motion of the waves. In fact, for the very high shear stresses, the wave amplitudes were between 2 and 5 % of the mean depth as shown in figure 4. These data were obtained by first averaging segments of the digitized depth-gauge output to obtain the mean depth in arbitrary units. The fluctuations were obtained by subtracting the mean from the value of the signal at each time. The r.m.s. value was then calculated in the usual way. Since the depth-gauge response was linear over small displacements, the r.m.s. values were independent of an absolute depth-gauge calibration. The calibration constant cancelled out when the ratios of fluctuations to their means were formed.

It appears that the waves were not only stable in the supersonic case, but were not large enough (0·0002 cm) to be called roughness elements. Data were also obtained for the wavelengths and the wave speeds for the case of laminar boundary layers. These data are presented in § 4. This information, when coupled with the wave amplitude, can provide input to improved heat-transfer models of ablating surfaces and transpiring layers.

Spectral analysis of the depth-gauge data permitted determination of the characteristic frequencies of the wave patterns. The frequency was found to be insensitive to the liquid Reynolds number but sensitive to changes in the external

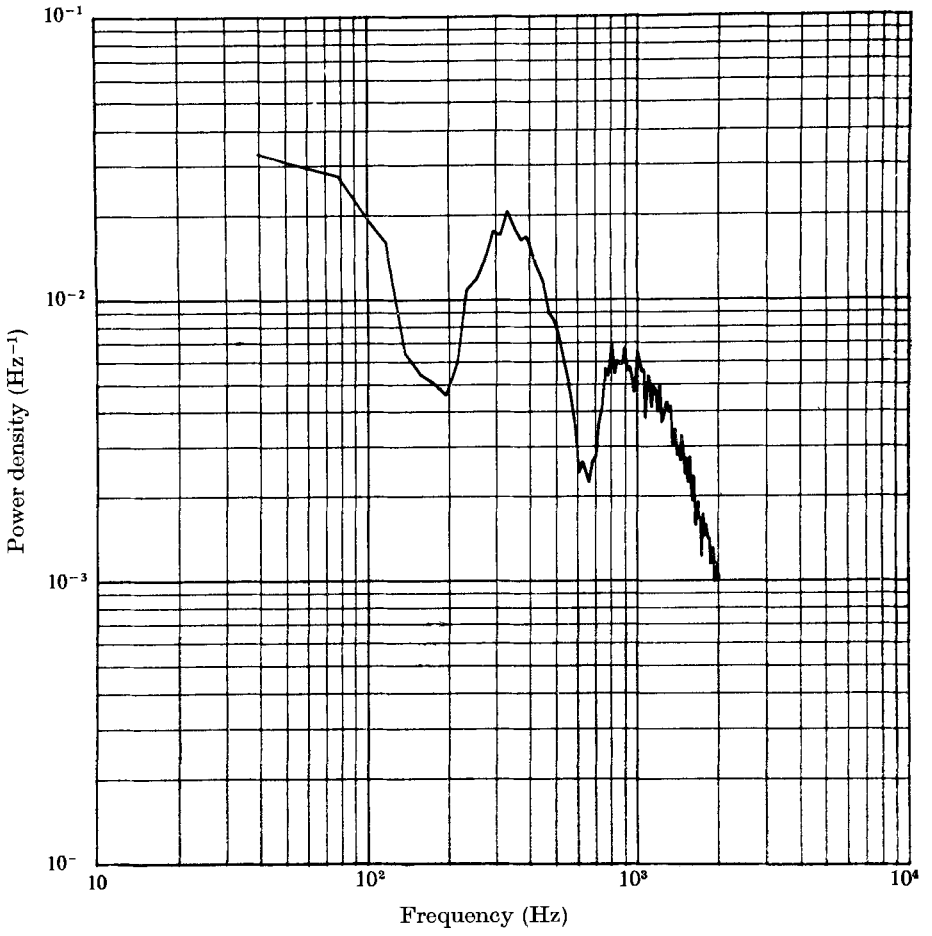

FIGURE 6. Power density *vs.* frequency for a turbulent boundary layer. Liquid Reynolds number is 5·7.

flow, as seen in figure 5. The turbulent boundary layers showed two energy peaks for every test except those for very low Reynolds numbers. An example of this is shown in figure 6. This figure is a computer-generated plot of power density versus frequency obtained directly from a Fourier spectral analysis of the depth-gauge output. The second peak in energy could be due to an interaction with the turbulent fluctuations in the boundary layer or to a second-harmonic resonant condition on the interface. It also could be due to resonance with the supersonic gas flow. This point will be discussed in § 4 in connexion with the nonlinear theory.

The results of Gold (1973) are qualitatively in agreement with ours, but the experiments differ in their details. He used both wedge and cone-shaped models, but his coolant was pure water. Therefore the only way he could change the liquid Reynolds number was by changing the flow rate. Also, he used a photo-densitometer to determine the wave characteristics, while we used an end-effect capacitance and motion pictures. Therefore he did not present frequency or

wavenumber data. He observed no liquid entrainment, in agreement with our observations, and he observed a reduction of the wave amplitude with increasing gas shear, which was also observed in the present experiments. The main difference between these two sets of experiments is that Gold did not concentrate on the interface characteristics; instead he concentrated on the behaviour of the heat-transfer rates and on the angle-of-attack effects.

4. Comparison of analytical and experimental results

The motion of the gas parallel to the liquid layer produces two important effects on the liquid. The first is the exertion of a mean shear stress at the liquid/gas interface, which in turn establishes a mean velocity profile in the liquid. The second is the exertion of pressure and shear-stress perturbations on the liquid owing to the appearance of waves on the interface. Whereas the former effect can be stabilizing or destabilizing depending on a number of conditions, the latter leads to pressure-perturbation (Kelvin–Helmholtz) and shear-perturbation (Craik–Benjamin) instability mechanisms. In this section, we discuss stability theories and compare them with the experiments. First we consider the linear theories and then the nonlinear theories.

Linear theories

In determining the linear stability of the liquid film, we need to model the gas motion. If the gas is inviscid and subsonic and flowing parallel to the undisturbed surface with a uniform mean velocity, the pressure perturbation is 180° out of phase with the surface wave. In this case, the gas pushes down at the troughs and sucks at the crests of the wave, thereby feeding energy to the disturbance in the liquid layer. In this model, the effect of the axial component of the pressure perturbation is cancelled. A different situation arises if the external flow is inviscid and supersonic. In this case, the pressure perturbation is in phase with the wave slope, giving rise to maximum energy transfer from the gas to the liquid through supersonic wave drag.

Since the gas is viscous, the mean-flow velocity decreases from its supersonic free-stream value at the edge of the boundary layer to a small velocity (nearly equal to that of the mean liquid surface) as shown in figure 7. Then the phase of the pressure perturbation exerted on the gas by the liquid interface lies between the inviscid subsonic and supersonic values. Since the experimental results show that the liquid surface velocity and the wave speeds are very small compared with the gas free-stream velocity, one can assume the liquid surface to be stationary in calculating the pressure and shear perturbations. Moreover, since the gas Reynolds numbers based on the observed wavelengths are large, the mean flow can be assumed to be parallel. Bordner, Nayfeh & Saric (1975) showed that including the effects of the mean-flow profile strongly changes the stability characteristics of the liquid film. They also showed that including the effects of viscosity in calculating the shear and pressure perturbations changes the film stability characteristics, but to a lesser degree. Their calculations were made for linear mean profiles within the disturbance boundary layer. However,

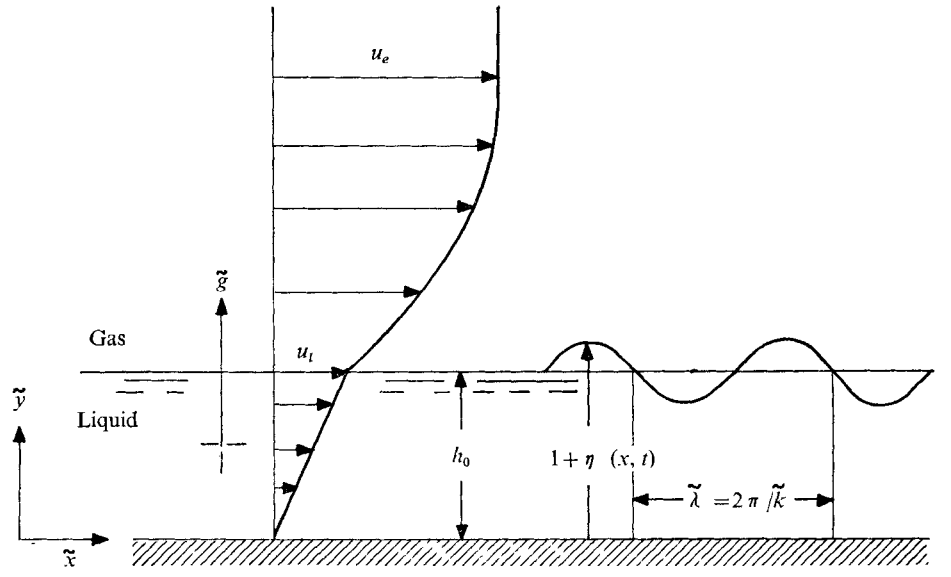

FIGURE 7. Flow geometry. Basic state and disturbance.

Lekoudis, Nayfeh & Saric (1976) showed that the aforementioned assumption is not valid for turbulent flows, because the disturbance boundary-layer thickness is not small when compared with the mean boundary-layer thickness. Therefore we determined the linear stability characteristics of the liquid films by taking into account the gas mean-flow profile and the gas viscosity without any restriction on the size of the disturbance boundary layer.

According to the linear analysis, the observed waves should correspond to the ones with maximum amplification rates. Although the linear analysis is in good agreement with the subsonic case, it is in poor agreement with the supersonic case.

The results of all linear models show that a liquid film adjacent to a supersonic stream is much more unstable than a liquid film adjacent to a subsonic stream, in qualitative disagreement with the present and past experimental data.

Nonlinear theories

The experiments show a stable, though not flat, liquid layer in the supersonic case, contrary to the prediction of the linear theory. This behaviour can be explained by using the nonlinear theory of Nayfeh & Saric (1971). They assumed the liquid film to be quiescent and the gas to be inviscid and moving with a uniform velocity parallel to the liquid film. Nonlinear disturbances were taken into account in both the gas and the liquid, and the nonlinear motion of the interface was analysed. Their nonlinear results show that unstable linear disturbances continue to be unstable in the subsonic case, but achieve steady-state amplitudes in the supersonic case, in qualitative agreement with the experimental observations.

Subsequently, Nayfeh & Saric (1973) removed the assumption that the liquid was initially quiescent by taking the liquid velocity profile (i.e. the mean shear stress exerted by the gas on the interface) into account. However, they neglected the gas viscosity and mean-flow profile in calculating the pressure perturbations exerted by the gas on the interface. In spite of the success of this new model in predicting the existence of the experimentally observed periodic waves, it cannot predict quantitatively the observed wavelengths and the corresponding amplitudes. Therefore, this model was improved by Bordner & Nayfeh (1974) by including the effects of gas viscosity and the mean-flow profile in calculating the pressure and shear perturbations exerted by the gas on the gas/liquid interface. In the remainder of this section, we outline their analysis and use it to correlate the data.

Assuming dispersive waves, they expanded the wave amplitude in a Fourier series as

$$\eta(x,t) = \epsilon\eta_1(t)\exp(ix) + \epsilon^2\eta_2(t)\exp(2ix) + \epsilon^3\eta_3(t)\exp(3ix) + \text{c.c.} + O(\epsilon^4), \tag{1}$$

where c.c. stands for the complex conjugate of the preceding terms and

$$d\eta_1/dt = -i(c_1 + \epsilon^2 c_2)\,\eta_1 + 4i\epsilon^2 c_3\,\eta_1^2\bar{\eta}_1, \tag{2}$$

$\bar{\eta}_1$ being the complex conjugate of η_1. Moreover, they represented the liquid disturbance stream function and the gas disturbance pressure in the form

$$\begin{aligned}\psi(x,y,t) = {} & \epsilon\eta_1\phi_1(y)\exp(ix) + \epsilon^2\{[\eta_2\phi_2(y) + \eta_1^2\phi_3(y)]\exp(2ix) \\ & + \tfrac{1}{2}\eta_1\bar{\eta}_1\phi_4(y)\} + \epsilon^3\{[\bar{\eta}_1\eta_2\phi_5(y) + \eta_1^2\bar{\eta}_1(\phi_6(y) + 4c_3\tilde{\phi}_6(y)) \\ & + \eta_1(\phi_7(7) + c_2\tilde{\phi}_7(y))]\exp(ix) + \text{h.h.}\} + \text{c.c.} + O(\epsilon^4),\end{aligned} \tag{3}$$

$$\begin{aligned}p(x,y,t) = {} & \epsilon\eta_1 p_1(y)\exp(ix) + \epsilon^2\{[\eta_2 p_2(y) + \eta_1^2 p_3(y)]\exp(2ix) + \tfrac{1}{2}\eta_1\bar{\eta}_1 p_4(y)\} \\ & + \epsilon^3\{[\eta_2\bar{\eta}_1 p_5(y) + \eta_1^2\bar{\eta}_1 p_6(y)]\exp(ix) + \text{h.h.}\} + \text{c.c.} + O(\epsilon^4),\end{aligned} \tag{4}$$

where h.h. stands for higher harmonics. Furthermore, they expressed the other gas variables (u, v, T) in forms similar to (4).

Substituting these equations into the disturbance equations and separating variables, they determined the equations describing the p_n, u_n, v_n and T_n. Assuming the gas mean-flow profiles to be linear within the disturbance boundary layer, they used the method of matched asymptotic expansions to determine the appropriate boundary conditions next to the interface for the p_n. Using these conditions together with the inviscid boundary conditions away from the interface, they solved numerically for the p_n and determined the pressure and shear perturbations exerted by the gas on the interface.

With the pressure and shear perturbations known, they substituted (1)–(4) into the equation describing the liquid disturbance stream function, the wall boundary condition, the equation of continuity of normal and tangential stresses at the interface and the kinematic condition at the interface. Separating variables in the resulting equation and boundary conditions, they obtained the problems describing η_2 and the ϕ_n. Solving these problems gives the c's and hence the stability characteristics of the interface.

Equation (2) shows that the stability of the interface depends on the signs and the relative magnitudes of the imaginary parts of $c_1 + \epsilon^2 c_2$ and c_3. The linear

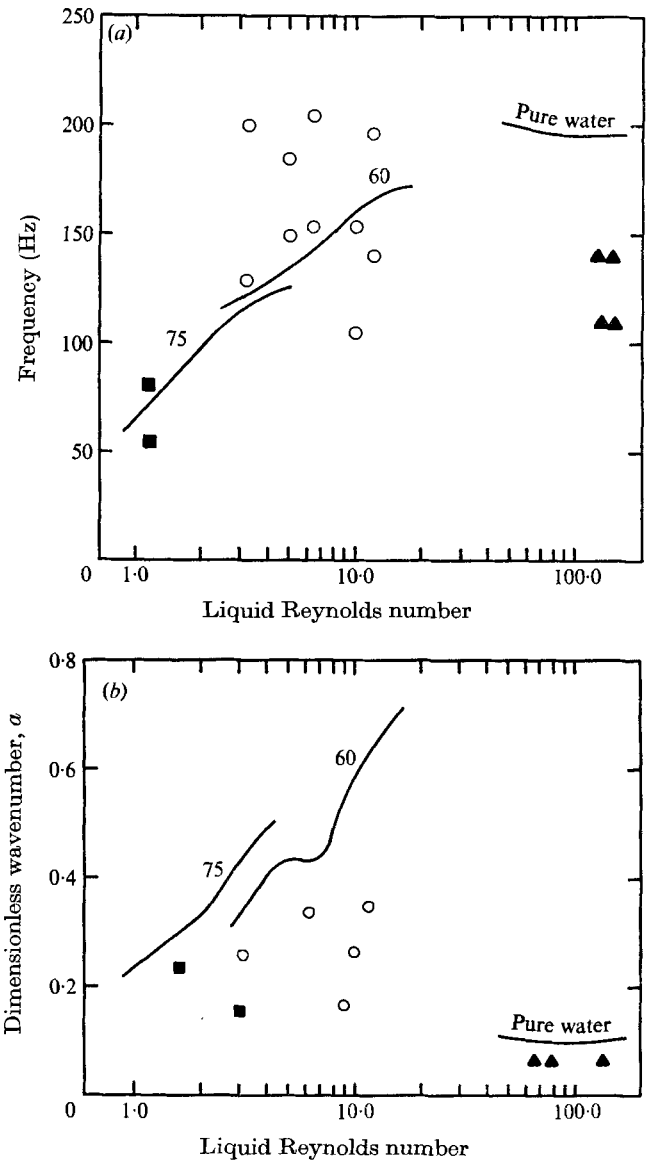

FIGURE 8. Comparison of predicted and observed (*a*) frequencies and (*b*) wavenumbers using the viscous nonlinear theory for the case of a laminar boundary layer. ——, theory; ■, 75 % glycerin; ○, 50 % glycerin; ▲, pure water. $\tau \equiv 130$ dynes/cm^2.

analysis predicts stability or instability depending on whether $\mathrm{Im}(c_1 + \epsilon^2 c_2)$ is negative or positive, while the effect of the nonlinearity is stabilizing or destabilizing depending on whether $\mathrm{Im}\ c_2$ is negative or positive.

As mentioned in the previous section, the observed frequencies do not correspond to the most amplified disturbances suggested by the linear theory. The nonlinear theory shows that these disturbances do not grow indefinitely, owing to the stabilizing effect of the nonlinearity, but achieve steady-state amplitudes.

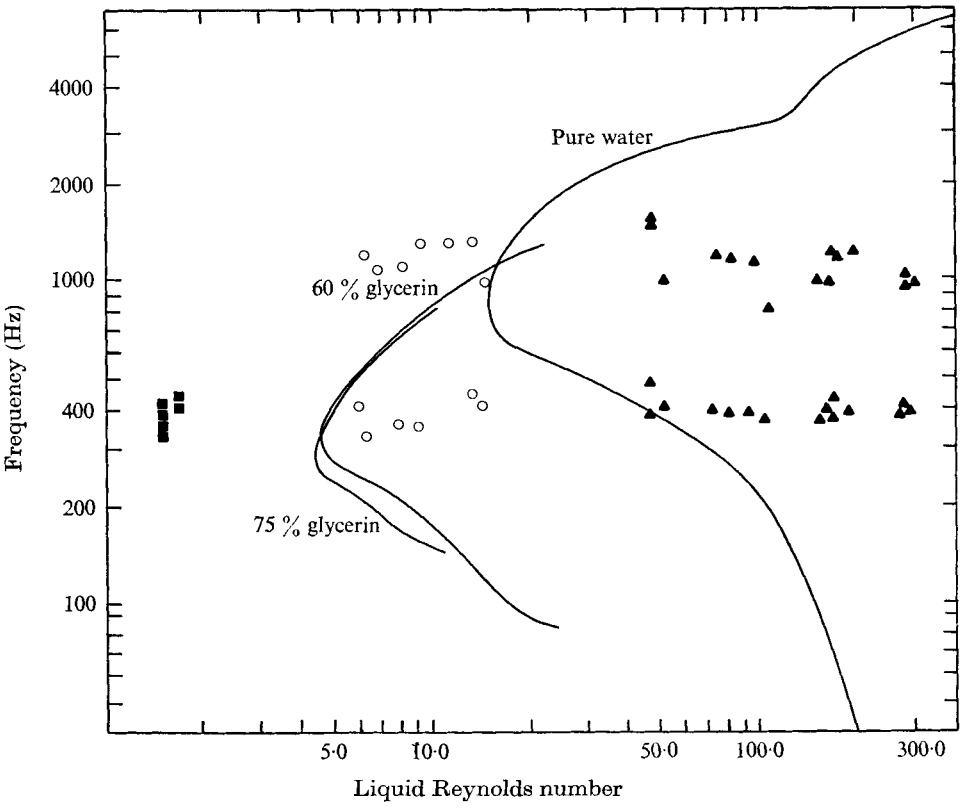

FIGURE 9. Comparison of predicted and observed frequencies using the viscous nonlinear theory for the case of a turbulent boundary layer. Notation as in figure 8. $\tau = 1800$ dynes/cm^2.

Moreover, the most amplified wave according to the linear theory does not have the largest steady-state amplitude. In fact, it is very much smaller than the steady-state amplitude of the wave corresponding to Im $c_3 \approx 0$. Therefore, we follow Bordner & Nayfeh (1974) and correlate our observed frequencies and wavenumbers with those corresponding to Im $c_3 = 0$.

For the case of laminar boundary layers, the predicted frequencies and wavenumbers agree closely with the new experimental data (figure 8). An important result is that for small wavenumbers we observe positive nonlinear amplification rates, which means growing waves, contrary to the experimental observations. By examining this region of wavenumbers more carefully, we found a second zero of the nonlinear amplification rate. However, it occurs at a frequency and a wavenumber too small to be measured.

For the case of turbulent boundary layers, we made the 'quasi-laminar' assumption (i.e. that the disturbances and the turbulent fluctuations are uncorrelated). The nonlinear theory predicts two maximum amplitude waves; that is, there are two frequencies for which Im $c_3 = 0$. This is in agreement with the experiments, which show two dominant frequencies for each run. The variation of the predicted frequencies with the liquid Reynolds number is shown in figure 9 along with the observed frequencies. Also, the variation of the predicted wave-

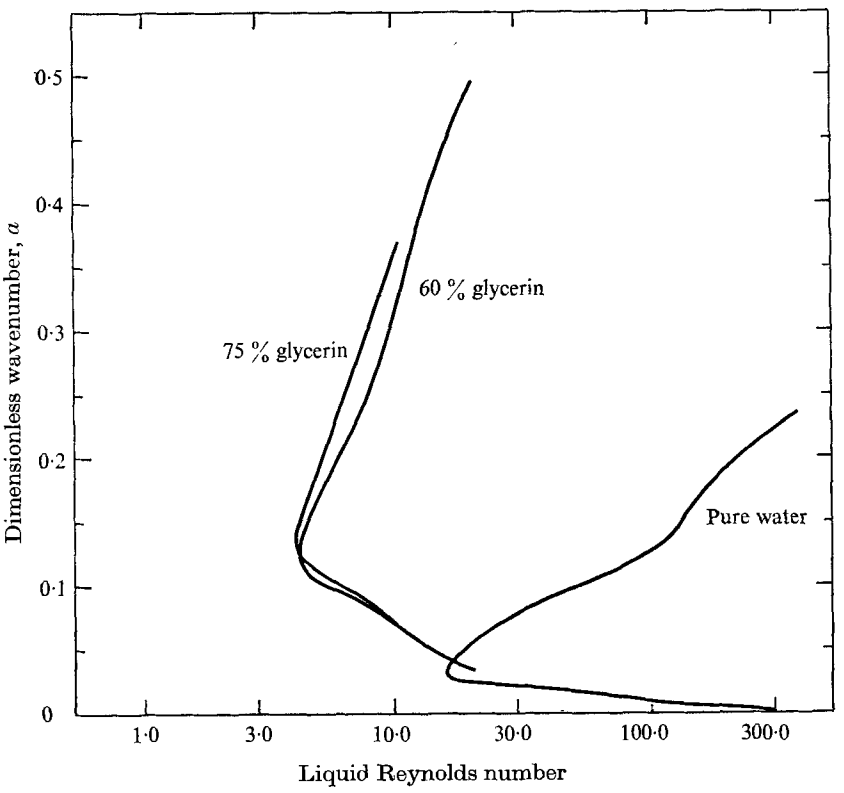

FIGURE 10. Predicted wavenumbers for the case of a turbulent boundary layer. $\tau = 1800$ dynes/cm^2.

numbers with the liquid Reynolds number is shown in figure 10. Because of the thinness of the liquid films, the disturbance wavelengths were very small. Consequently, we are not able to determine the wavelengths accurately from the data.

In spite of the success of the present nonlinear analysis in predicting the observed frequencies, it cannot predict the observed amplitudes quantitatively.

5. Conclusions

The stability of liquid films adjacent to supersonic streams was investigated experimentally. It was found that the flat liquid/gas interface is unstable. However, stable finite amplitude waves were observed on the interface. The observed frequencies cannot be correlated by using linear theories but can be correlated by using nonlinear theories, which predict the existence of stable waves having finite amplitudes.

The experimental portion of this work was done while one of the authors (W.S.S.) was with Sandia Laboratories. We should like to express our appreciation to Dr Victor Zakkay and his staff at NYU and to Mr A. A. Trujillo and Mr

J. L. Banker at Sandia for their help and interest in the programme. This work was supported by the U.S. Energy Research and Development Administration and by the Fluid Dynamics Program of the Office of Naval Research.

REEFRENCES

ANDERSON, L. W. & KENDALL, R. M. 1969 Boundary layer integral matrix procedure. *Rep. Kirtland Air Force Base, New Mexico*, no. AFWL-TR-69-114, vol. I, II.

BORDNER, G. L. & NAYFEH, A. H. 1974 Nonlinear stability of a liquid film adjacent to a viscous supersonic stream. *Tech. Rep. Virginia Polytech. Inst. & State Univ., Blacksburg*, no. VPI-E-74-11.

BORDNER, G. L., NAYFEH, A. H. & SARIC, W. S. 1975 Stability of liquid films adjacent to compressible streams. *Z. angew. Math. Phys.* **26**, 771.

CHAPMAN, D. R. & LARSON, H. K. 1962 Aerodynamic evidence pertaining to the entry of tektites in the earth's atmosphere. *N.A.S.A. Tech. Rep.* no. R-134.

GATER, R. L. & L'ECUYER, M. R. 1971 A fundamental investigation of the phenomena that characterize liquid film cooling. *Int. J. Heat Mass Transfer*, **13**, 1925.

GOLD, H. 1973 Surface fluid and boundary layer interaction aspects of transpiration cooled nosetip concepts. *Tech. Rep. Wright-Patterson Air Force Base, Ohio*, no. AFML-TR-73-8.

GROSE, R. G. & KENDALL, R. M. 1970 The homogeneous BLIMP with liquid layer. *Rep. Aerotherm Corp., Mountain View, Calif.* no. 70–3.

KENDALL, R. M. & BARTLETT, E. P. 1972 Nonsimilar solution of the multi-component laminar boundary layer by an integral-matrix method. *A.I.A.A. J.* **6**, 1089.

LEKOUDIS, S. G., NAYFEH, A. H. & SARIC, W. S. 1976 Compressible boundary layers over wavy walls. *Phys. Fluids*, **19**, 514.

MARSHALL, B. W. & TIEDERMAN, W. G. 1972 A capacitance depth gauge for thin liquid films. *Rev. Sci. Instr.* **43**, 544.

MUIR, J. F. & TRUJILLO, A. A. 1972 Experimental investigation of the effects of nose bluntness, freestream unit Reynolds number, and angle of attack on cone boundary layer transition at a Mach number of 6. *A.I.A.A. Paper*, no. 72–216.

MUIR, J. F. & TRUJILLO, A. A. 1974 Comparison of boundary layer transition measurements obtained in two wind tunnel facilities. *A.I.A.A. Paper*, no. 74-626.

NAYFEH, A. H. & SARIC, W. S. 1971 Nonlinear Kelvin–Helmholtz instability. *J. Fluid Mech.* **46**, 209.

NAYFEH, A. H. & SARIC, W. S. 1973 Nonlinear stability of a liquid film adjacent to a supersonic stream. *J. Fluid Mech.* **58**, 39.

SARIC, W. S. & MARSHALL, B. W. 1971 An experimental investigation of the stability of a thin liquid layer adjacent to a supersonic stream. *A.I.A.A. J.* **9**, 1546.

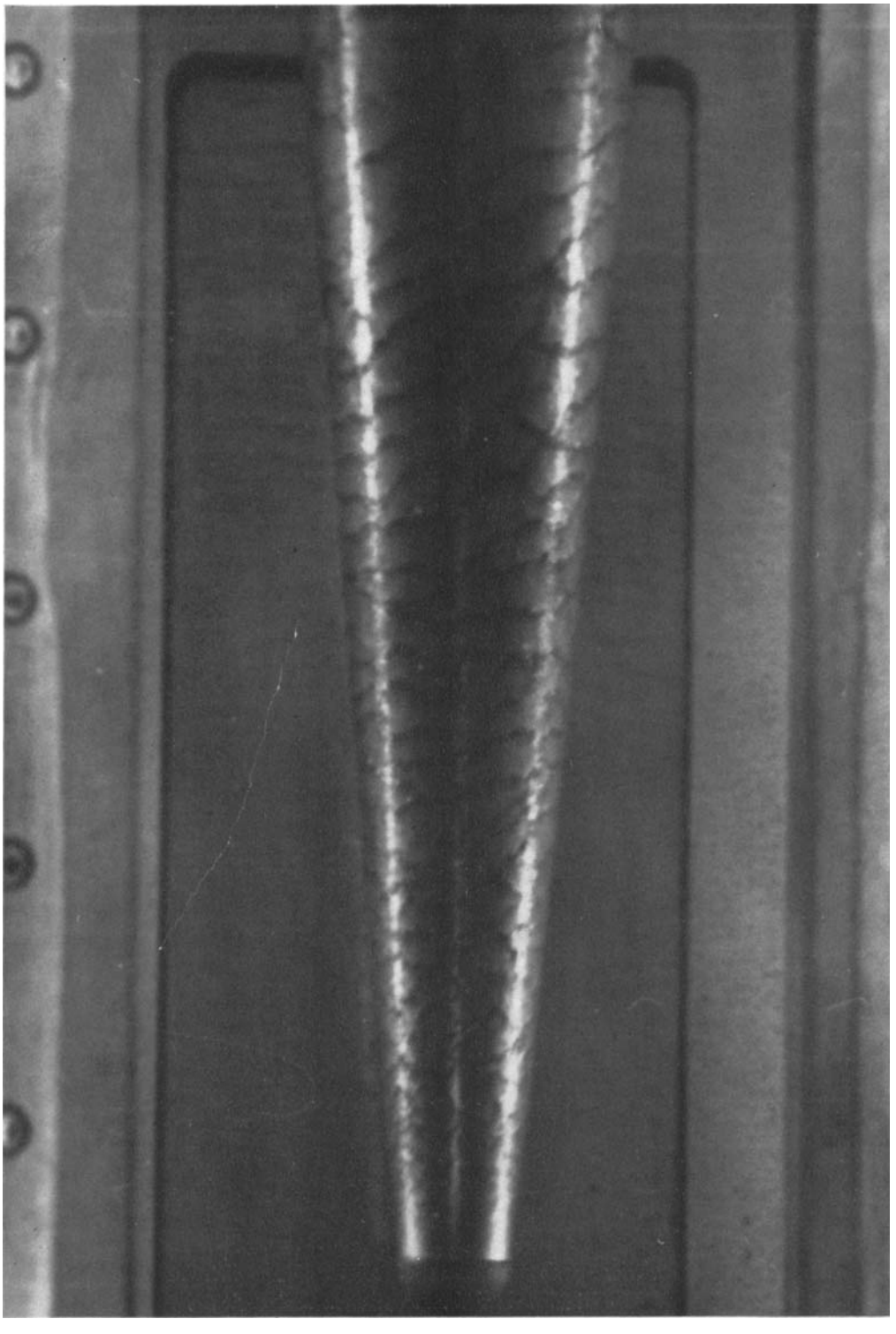

FIGURE 2. Supersonic flow over a water film. Laminar boundary layer and liquid Reynolds number of 80.

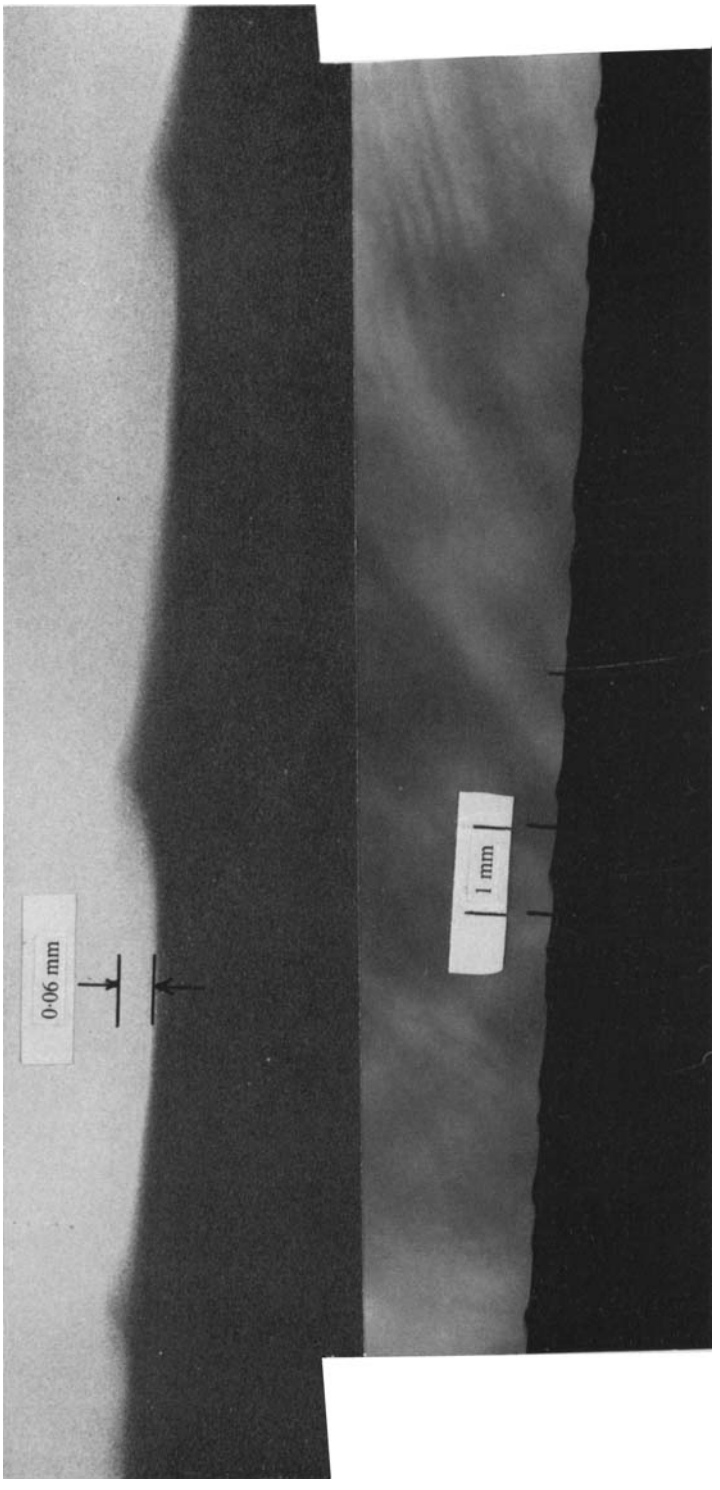

FIGURE 3. Spark photomicrograph of wave profile. Turbulent boundary layer over 75 % glycerin–water mixture. Upper photo, 100 × 1; lower photo, 7 × 1. 1. Flow is from left to right.